SCIENTIFIC REPORTS
nature research

OPEN

Arrangement optimization of water-driven triboelectric nanogenerators considering capillary phenomenon between hydrophobic surfaces

Hong Ryul Park[1,4], Jeong-Won Lee[1,4], Dong Sung Kim[1], Jae-Yoon Sim[2], Insang Song[3] & Woonbong Hwang[1*]

The rise in environmental issues has stimulated research on alternative energy. In this regard, triboelectric generation has received much attention as one of several new alternative energy sources. Among the triboelectric generation methods, solid-liquid triboelectric nanogenerators (SLTENGs) have been actively investigated owing to their durability and broad applicability. In this paper, we report on the optimum arrangement of SLTENGs to increase the generation of electrical energy. When hydrophobic SLTENGs are arranged in parallel with a specific intervening gap, the friction area between the water and the surface of the SLTENGs is changed owing to the different penetration distances of water between them. This difference affects the amount of triboelectricity generated; this change in the water contact area is caused by the capillary phenomenon. Therefore, we investigated the effect of the gap on water penetration and formulated an optimum arrangement to achieve optimum electricity generation efficiency when multiple SLTENGs are contained in a limited volume. The proposed optimum arrangement of SLTENGs is expected to have high utilization in energy harvesting from natural environment sources such as wave energy or water flow.

Nowadays, environmental issues such as global warming and climate change have become severe owing to the indiscriminate use of fossil energy. Moreover, the price of fossil energy will increase steadily because it is a finite resource. Therefore, many researchers have endeavoured to develop alternative green energies using sunlight, wind, tide, geothermal heat, and the like[1–10]. Among alternative energies, triboelectric nanogenerator (TENG) has received much attention in academia. TENG is a new invention that harvests energy using triboelectricity, which is common in our lives. Triboelectrification, also called contact electrification, is a common phenomenon that occurs when two different materials are in contact with each other[11–33]. Triboelectrification is commonly classified as solid-solid contact electrification and solid-liquid contact electrification[34,35]. Solid-solid contact electrification generally generates more energy than the solid-liquid type, but it is difficult to obtain sustainable energy from this owing to surface abrasion. In other words, the solid-liquid contact type can generate lower but continuous energy because the contact between solid and liquid does not cause abrasion of the solid surface. Therefore, studies have been carried out to amplify the amount of energy output through modification of the surface structure or stacking multiple TENGs[36–38]. Lee *et al.* reported on the effect of surface roughness on solid-liquid triboelectrification and proposed a method for fabricating high-performance solid-liquid type TENG[39–45]. When hydrophobic TENGs are stacked in parallel and submerged into a liquid, the penetration distance of the liquid into the gap between the TENGs varies owing to the capillary effect. Consequently, the effect leads to difference in the electricity generation.

[1]Department of Mechanical Engineering, Pohang University of Science and Technology (POSTECH), Pohang, 37673, Korea. [2]Department of Electrical Engineering, Pohang University of Science and Technology (POSTECH), Pohang, 37673, Korea. [3]Agency for Defense Development (ADD), Daejeon, 34186, Korea. [4]These authors contributed equally: Hong Ryul Park and Jeong-Won Lee. *email: whwang@postech.ac.kr

In this study, we developed an arrangement of TENGs that allows the most efficient energy output within a limited volume by considering the capillary effect. First, the gap between parallel-stacked solid-liquid TENGs (SLTENGs) that generates the maximum electrical output was investigated. Next, we analysed whether this optimal value of the gap is effective when the number of electrodes is varied within the limited volume. Through experimentation, the optimal arrangement of SLTENGs in a limited volume was determined for sustainable and increased electricity generation. The proposed arrangement can be regarded as a guide for increasing the electrical output of liquid-driven TENGs.

Experimental Section

Materials. Industrial aluminium plates (Al 5052, thickness: 1.0 mm) were purchased from Alfa Aesar, USA. Perchloric acid ($HClO_4$), ethyl alcohol (C_2H_5OH), oxalic acid ($C_2H_2O_4$), and n-hexane (C_6H_{14}) were obtained from SAMCHUN Chemicals, Republic of Korea. Heptadecafluoro-1, 1, 2, 2-tetrahydrodecyl trichlorosilane (HDFS) was supplied by JSI Silicone Co., Japan. Polytetrafluoroethylene (PTFE) was purchased from Du Pont, USA. All other chemicals were of analytical reagent grade and were used as received.

Fabrication and characterization. The proposed SLTENG was fabricated as follows. To eliminate the impurities and unevenness that influence contact electrification on industrial aluminium plates, the plates were polished in a mixture of perchloric acid and ethyl alcohol ($HClO_4$: C_2H_5OH = 1: 4 by volume) under a constant voltage of 20 V for 5 min using a computer power supply (Digital Electronics Co., DRP-92001DUS). The mixture was maintained at 7 °C during the polishing process by means of a circulator (Lab Companion, RW-0525G). After the polishing process, the plates were rinsed with deionized (DI) water and dried. To produce the anodized aluminium oxide (AAO) layer, which serves as a dielectric layer to hold the charge by triboelectrification, the as-prepared aluminium plates were anodized in 0.3 M oxalic acid solution maintained at 25 °C under a constant voltage of 50 V for 20 min using the computer power supply[39,46]. After the anodizing process, the plates were rinsed with DI water and dried. The anodized aluminium plates were dipped in a mixture of n-hexane and HDFS with volumetric ratio of 1000:1 for 10 min, followed by drying at 60 °C for 6 h. Then, PTFE was added to the surface to form an over-coating of the PTFE layer to cause the surface to become negatively charged in the triboelectric series. The plates were then washed with DI water and dried in a stream of air.

A field emission scanning electron microscope (FESEM; JEOL JSM-7401F, Japan) was used to observe the anodized Al surface and to measure the thickness of the anodized layer. The contact angle (CA) was measured with 5-μl water droplets using a CA measurement system (SmartDrop_Lab HS, FEMTOFAB, Republic of Korea). The average CA value was obtained by measuring each sample at a minimum of three different positions at room temperature. The optical images of the droplets were obtained using a digital camera.

Electrical output measurement. The fabricated SLTENGs were vertically mounted on an electrodynamic shaker (LABWORKS) and another electrode was attached to a beaker and placed below the shaker. The beaker was filled with 600 ml of DI water. The SLTENGs were then repeatedly dipped in water at a frequency of 2 Hz and dipping depth of 1 cm. The energy generated from water-solid contact electrification was analysed by measuring the output current and output voltage under the load resistance of 10 MΩ using an oscilloscope (DS1000Z, Rigol) and low-noise current pre-amplifier (SR570, Stanford Research Systems)[39].

Results and Discussion

Water-solid contact electrification of SLTENG. When the sliding contact electrification occurs, the charge and voltage follow the formula:

If the immersed depth is defined as x, the total charge (Q) is given by

$$Q = \sigma \times A_{contact} = \sigma w x, \tag{1}$$

where σ is the surface charge density and w is the width of the SLTENG. With regard to the relative interfacial velocity ($v_r(t)$), the output current (I) can be expressed as

$$I = \frac{dQ}{dt} = \sigma w \frac{dx}{dt} = \sigma w v_r(t) \tag{2}$$

The output voltage (V) can be expressed as

$$V = \frac{\sigma dx}{\varepsilon_0 \varepsilon_r (l - x)}, \tag{3}$$

where d and l are the effective dielectric thickness and the total friction length, respectively; ε_0 and ε_r are the dielectric constant of vacuum and relative permittivity of the dielectric material, respectively[46,47].

In triboelectric energy generation, definite contact and separation, and large contact area between liquid and the solid surface are critical factors for high electrical output. Therefore, a hydrophobic nano-hole structured surface of SLTENG was fabricated, as shown in Fig. 1(a). The surface roughness and impurities of bare aluminium were flattened and cleaned by electropolishing (Fig. 1(b,c)). The removal of surface impurities slightly enhanced the hydrophilicity (Fig. 1(a-I,a-II)). Through the subsequent anodization process, a superhydrophilic Al_2O_3 surface with evenly distributed 20-nm nanoholes was fabricated (Fig. 1(a-III,d)). Both the HDFS and the PTFE self-assembled monolayer (SAM) coatings chemically modify the surface and make it hydrophobic without making any changes to the surface structures. Although the SAM coating of HDFS can solely function as a hydrophobic surface, the chain formation of PTFE, $-(CF_2-CF_2)_n-$, increases durability against abrasion caused by continuous sliding friction of water and the surface.

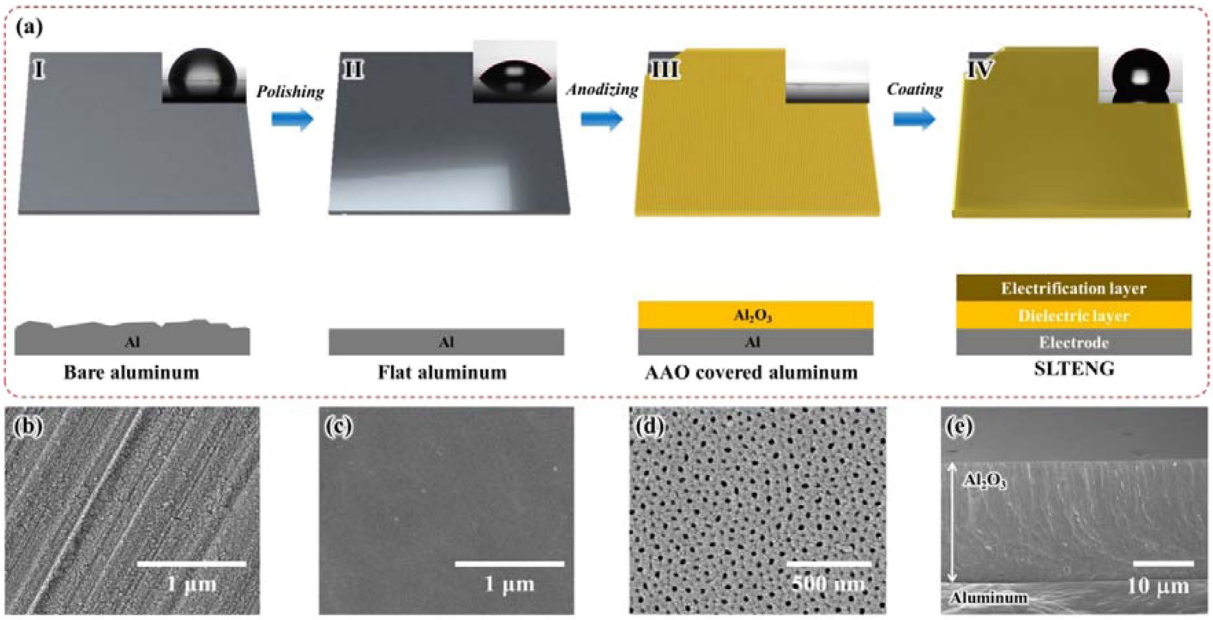

Figure 1. (**a**) Fabrication process of the solid-liquid triboelectric nanogenerator (SLTENG) with contact angles (CAs). Scanning electron microscopy (SEM) images of (**b**) bare aluminum, (**c**) electropolished aluminum, (**d**) anodized aluminum. (**e**) Cross-sectional SEM image of Al_2O_3.

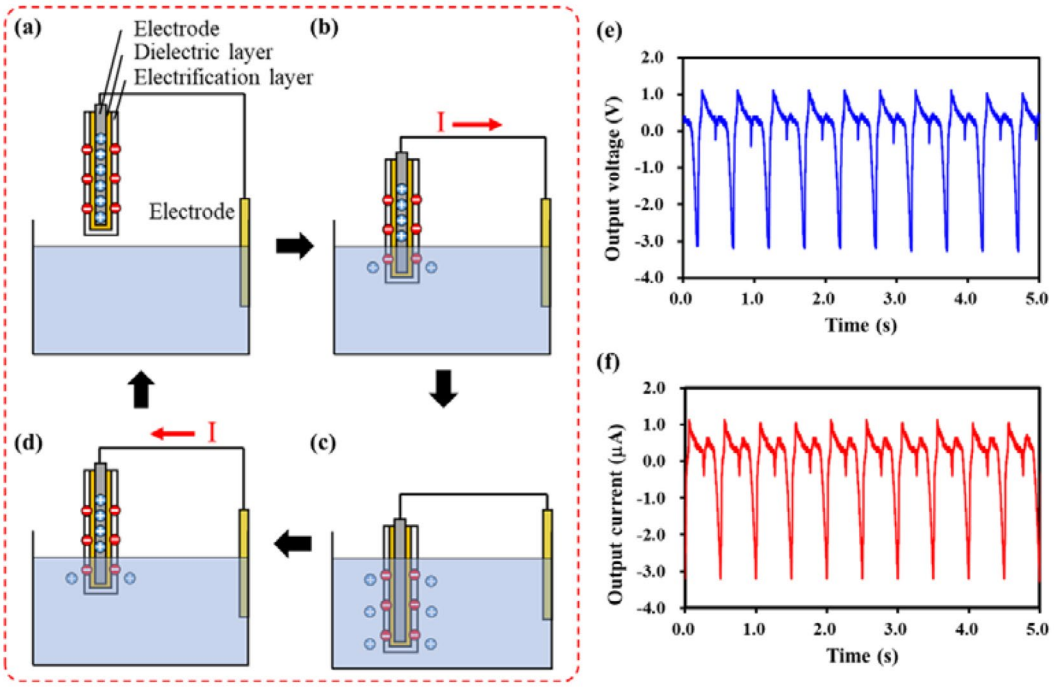

Figure 2. (**a**–**d**) Schematic of solid-liquid triboelectrification process of SLTENG. (**e**) Output voltage and (**f**) output current of single SLTENG.

The fabricated SLTENG comprised three layers: electrode, dielectric layer, and electrification layer (Fig. 1(a-IV)). The dielectric layer was the AAO layer of approximately 20-μm thickness, which provided insulation between liquid and the electrode (Fig. 1(e)). The electrification layer, which loses or gains electrons on contact, consisted of a PTFE coating. PTFE tends to be negatively charged in a triboelectric series. The SLTENG had a CA of 120°.

The simplified solid-liquid triboelectrification process of SLTENG is shown in Fig. 2. Before the SLTENG contacts with water, the entire system, including the SLTENG and water, is in a state of electrical equilibrium (Fig. 2(a)). When the SLTENG comes into contact with water, the electrification layer of the SLTENG and water

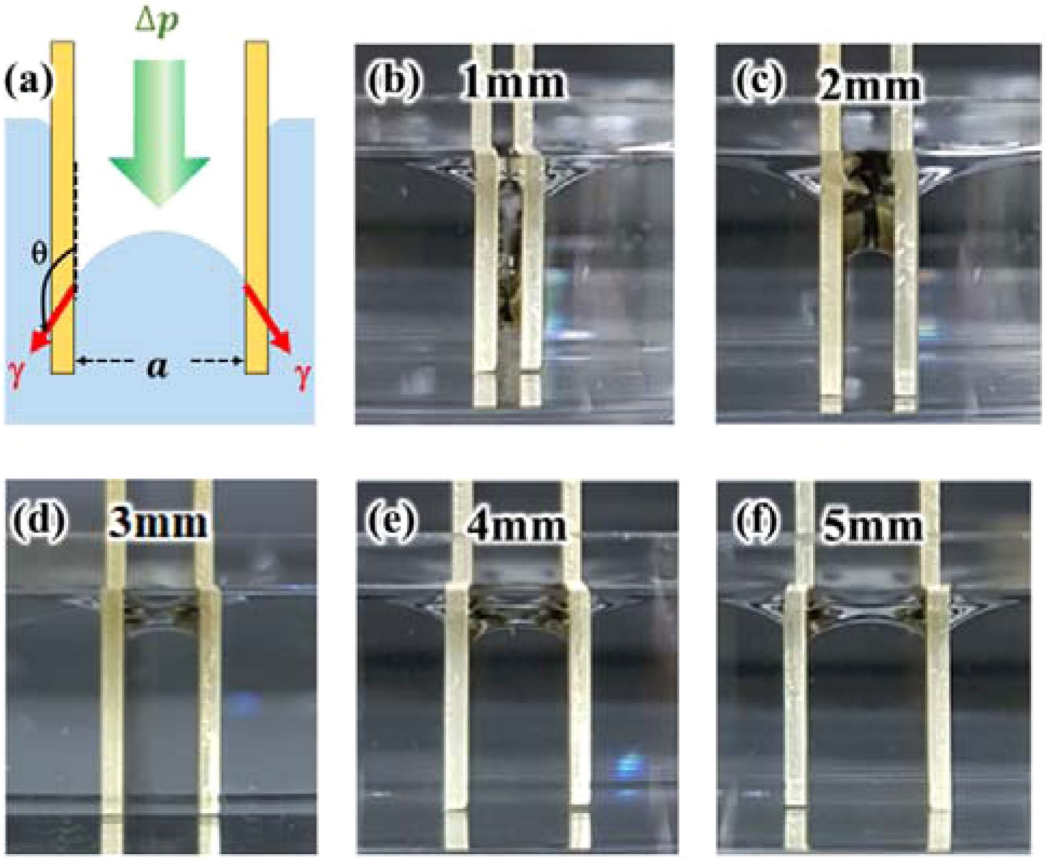

Figure 3. (**a**) Formation of capillary pressure between SLTENGs. (**b**–**f**) Optical images of water penetration with change in gap size from 1 mm to 5 mm.

are respectively electrified negatively and positively due to the triboelectric series and current flows from the SLTENG to water to maintain the electrical equilibrium (Fig. 2(b)). When fully dipped in water, the SLTENG and water are in electrical equilibrium (Fig. 2(c)). When the SLTENG is out of the water, the surface of the SLTENG and water are electrified and current flows reversely (Fig. 2(d)). When the SLTENG is fully out of water, the state is the same as in Fig. 2(a) and the process is repeated. The electrical output measurements of a single SLTENG are shown in Fig. 2(e,f). The output voltage and current of a single SLTENG are approximately 3 V and 3.2 μA, respectively, at a frequency of 2 Hz and amplitude of 1 cm using the electrodynamic shaker. The power variation by frequency and amplitude is shown in Fig. S1. The amount of electricity generated differs according to the frequency and amplitude, but we applied 2 Hz and 1 cm as the natural wave environment in this experiment. A parallel arrangement with a specific gap was devised to increase the amount of electricity generation.

Gap analysis between SLTENGs considering capillary effect. An experimental model was devised to analyse the amount of electrical output based on the size of the gap between the SLTENGs arranged in parallel. Increasing in the number of electrodes resulted in increased electricity generation, but the volume of the entire TENG system also increased. In order to reduce the volume, it is essential to apply a narrower gap when multiple SLTENGs are stacked. However, the narrow gap increases the capillary pressure, which resists the penetration of water into the gap between the SLTENGs because of their hydrophobic property (Fig. 3(a)). Thus, the surface contact area with the water decreases and this leads to decrease in the electrical output. Capillary pressure is the difference in the pressures at the interface between two immiscible fluids such as water and air (Eq. (4)).

The capillary pressure Δp is expressed as[48],

$$\Delta p = \frac{2\gamma cos\theta}{a}, \tag{4}$$

where a, γ, and θ are the radius of the capillary, the liquid/vapor interfacial tension, and the contact angle of the material, respectively. As the gap decreases, the capillary pressure increases. In the case of a hydrophobic surface, the pressure is negative, which prevents water from penetrating the capillary. In this experiment, the gap is the sole parameter because the applied surfaces have the same wetting properties. As the gap between the hydrophobic plates varies, the height of the water in the gap varies owing to negative capillary pressure.

To identify the quantity of water that penetrates between the hydrophobic plates, stacked SLTENGs separated by a specific gap were immersed in a circular chalet with 1-cm-deep water. The heights to which water had

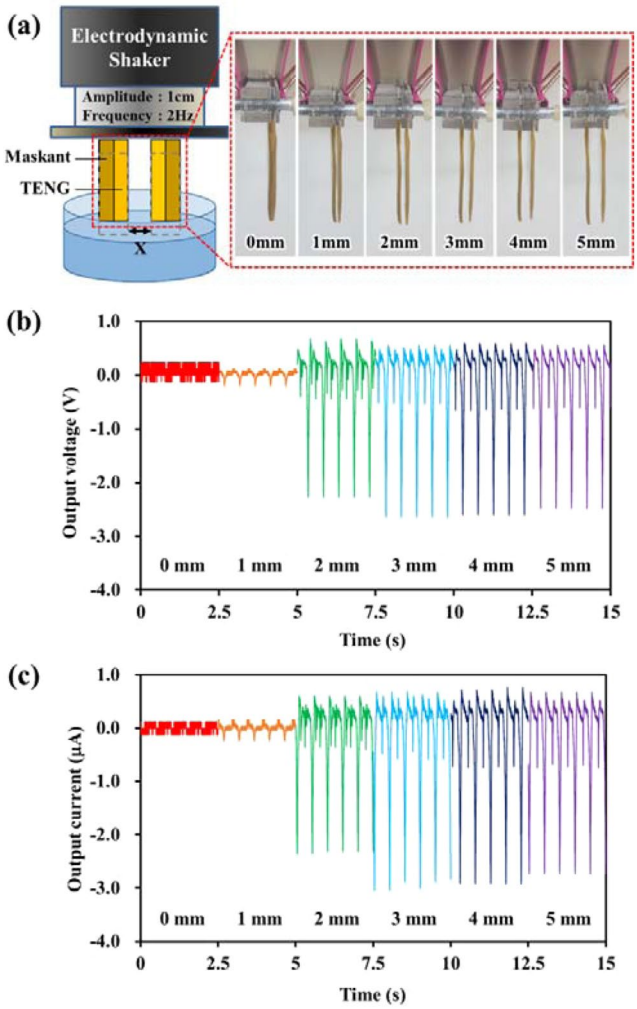

Figure 4. (**a**) Experimental setup for gap optimization. (**b**) Output voltage and (**c**) output current by altering the gap between two SLTENGs.

penetrated between the plates were observed while increasing the gap between two surfaces from 1 mm to 5 mm (Fig. 3(b–f)). As shown in the figure, the equilibrium of force is reached at the lower water level between the plates than outside the plates because of the higher capillary pressure. The penetration height of water between the plates is the lowest at the gap of 1 mm, which means that the capillary pressure is the maximum at 1 mm. As the gap increases gradually, the water level also increases. After 3 mm, it becomes almost equal to the height of the water outside the plates. This is because the influence of the capillary pressure generated between the plates is negligible, irrespective of the gap. Computer Aided Engineering (CAE) was performed to verify the height of water penetration between SLTENGs due to capillary phenomenon. A commercial program, ANSYS Fluent, was used for the analysis, and the result showed the same tendency of water penetration (Fig. S2). Also, the same tendency was observed under the real-time condition (Fig. S3).

Gap optimization between two SLTENGs. Figure 4(a) shows the actual experimental setup and illustration of the gap optimization between two SLTENGs. To investigate the change in electrical generation with gap between two SLTENGs, the sides and back of the fabricated SLTENGs were insulated using a maskant. The insulation was applied to obtain the electricity generated only from the inner gap between the two SLTENGs. The gap between the two SLTENGs was varied from 0 mm to 5 mm and their electrical energy evaluated at a frequency of 2 Hz and amplitude of 1 cm using the electrodynamic shaker.

The results are shown in Fig. 4(b,c). When the gap between the SLTENGs was 0 mm, the electrical output was virtually zero because there was no contact with water. When the gap was 1 mm, the measured generation value was 0.2 V and 0.25 μA. In spite of the 1-mm gap between the SLTENGs, the power generation was very low. Because the capillary pressure, which is inversely proportional to the gap, interfered with the penetration of water, only a small contact area existed between the SLTENG surface and water. In other words, the electrical output increased with the gap size because of the lowering of the capillary pressure. As a result, the power output gradually increased as the gap increased from 0 mm to 3 mm, and the maximum electrical output was 2.6 V and

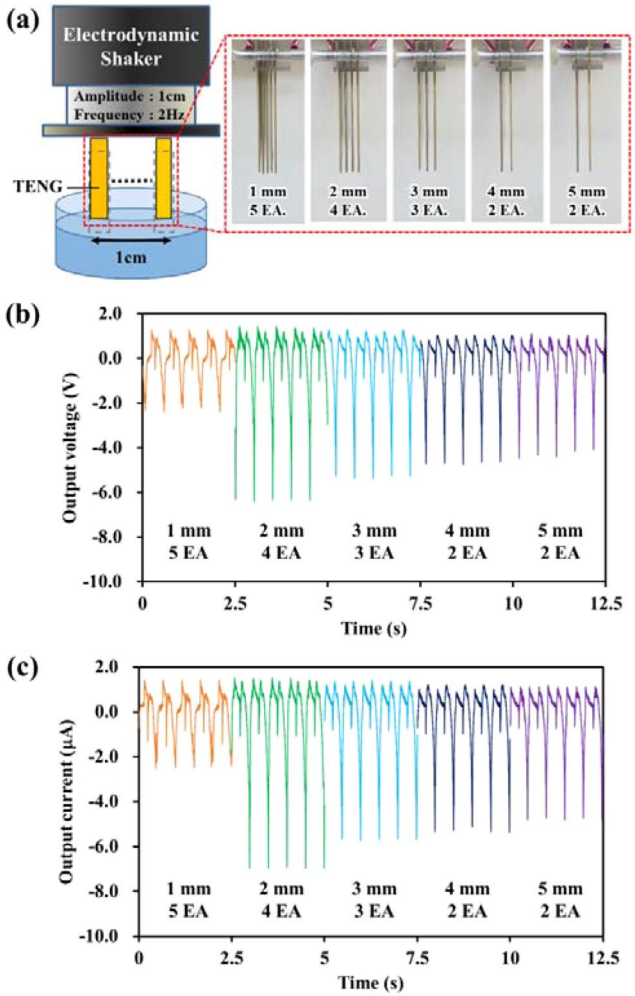

Figure 5. (**a**) Experimental setup for areal density optimization. (**b**) Output voltage and (**c**) output current by altering the gap between the SLTENGs within a limited volume.

3 μA at a gap of 3 mm. This amount was slightly lower than the energy output of the single SLTENG because the sides and back of the SLTENGs were insulated by the maskant. The measured energies at gaps of 4 mm and 5 mm were almost the same as that at the 3-mm gap. It is considered that the capillary pressure no longer affects water penetration when the gap increases beyond 3 mm, as observed in the previous gap analysis experiment. Therefore, the 3-mm gap between two SLTENGs is the best gap for maximum electrical output.

Areal density optimization in limited volume. The number of electrodes is also a critical factor for arranging electrodes efficiently with a specific gap within a limited volume. Therefore, it is necessary to study the dependence of power generation on the number of electrodes and the gap between the electrodes in a limited volume. Consequently, five electrodes with a 1-mm gap, four electrodes with a 2-mm gap, three electrodes with a 3-mm gap, and two pairs of electrodes with 4-mm and 5-mm gaps were placed within a limited distance of 1 cm (Fig. 5(a)). Other conditions for measurement were the same as in the gap optimization experiment.

The electrical outputs depending on the number of electrodes and the gap are shown in Fig. 5(b,c). Both output voltage and current were measured by a probe with an impedance of 10 MΩ. For reference, high-impedance probe measurement for open-circuit voltage was conducted and only the water penetration height was affected regardless of the contact area (Fig. S4). As shown in Fig. 5, the electrical outputs of the five electrodes with 1-mm gap are the lowest because the contact area of the SLTENGs with water is the smallest, as also shown in the gap optimization test. However, unlike in the previous test, the highest power occurs at the 2-mm gap. The power density can be expressed in watts, the product of voltage and current. Therefore, power density also follows the same trends of voltage and current, showing the highest amount of energy at 2 mm-gap. The highest power density was 8.84 $\mu W/cm^3$, which was over 7 times higher than the same volume of 1.15 $\mu W/cm^3$ with 1 mm-gap condition. This result shows that the number of electrodes has greater influence on the power generation than electrode spacing when water in the gap penetrates to a certain height in the limited volume. Therefore, for efficient enhancement of triboelectric power generation, it can be concluded that while increasing the number of SLTENGs, due consideration should be given to the limited volume and the capillary phenomenon.

Conclusions

In this paper, we proposed an optimum arrangement for SLTENGs for improving the power generation from solid-liquid triboelectrification. When multiple SLTENGs are arranged to increase the contact area with the liquid, a narrow gap between the SLTENGs needs to be avoided to allow water to penetrate into the gap. On the other hand, the gap size should not be excessively large to ensure high areal density considering the limited volume. Therefore, the optimum gap size for the highest efficiency of the SLTENGs was experimentally investigated. While 3 mm was the optimum gap size when considering solely the capillary phenomenon, the maximum power was generated at 2 mm-gap size considering the limited volume. Furthermore, although aluminium-based TENGs were used in this study, the applications of this study are not limited to the materials or the surface property. Rather, it can be applied to a variety of applications using water flow or wave power to generate a continuous electrical output, which is an advantage of solid-liquid TENG.

Received: 28 June 2019; Accepted: 8 November 2019;
Published online: 24 January 2020

References

1. Schiermeier, Q., Tollefson, J., Scully, T., Witze, A. & Morton, O. Electricity without Carbon. *Nature* **454**, 816–823 (2008).
2. Clery, D. Renewable energy. U.K. ponders world's biggest tidal power scheme. *Science* **320**, 1574 (2008).
3. Ku, M.-L., Li, W., Chen, Y. & Ray Liu, K. J. Advances in Energy Harvesting Communications: Past, Present, and Future Challenges. *IEEE Commun. Surv. Tutor.* **18**, 1384–1412 (2016).
4. Tian, B., Kempa, T. J. & Lieber, C. M. Single nanowire photovoltaics. *Chem. Soc. Rev.* **38**, 16–24 (2009).
5. Chen, J. *et al*. Micro-cable structured textile for simultaneously harvesting solar and mechanical energy. *Nat. Energy* **1**, 16138 (2016).
6. Wang, Z. L., Zhu, G., Yang, Y., Wang, S. & Pan, C. Progress in nanogenerators for portable electronics. *Mater. Today* **15**, 532–543 (2012).
7. Wang, X., Song, J., Liu, J. & Wang, Z. L. Direct-Current Nanogenerator Driven by UltrasonicWaves. *Science* **316**, 102–105 (2017).
8. Zhang, N. *et al*. A Wearable All-Solid Photovoltaic Textile. *Adv. Mater.* **28**, 263–269 (2016).
9. Lin, Z. *et al*. Broadband and three-dimensional vibration energy harvesting by a non-linear magnetoelectric generator. *Appl. Phys. Lett.* **109**, 253903 (2016).
10. Song, J. & Wang, Z. L. Piezoelectric Nanogenerators Based on Zinc Oxide Nanowire Arrays. *Science* **312**, 242–246 (2016).
11. Fan, F.-R., Tian, Z.-Q. & Wang, Z. L. Flexible triboelectric generator. *Nano Energy* **1**, 328–334 (2012).
12. Wang, Z. L. Triboelectric nanogenerators as new energy technology and self-powered sensors - principles, problems and perspectives. *Faraday Discuss.* **176**, 447–458 (2014).
13. Zi, Y. *et al*. Harvesting Low-Frequency (<5 Hz) Irregular Mechanical Energy: A Possible Killer Application of Triboelectric Nanogenerator. *ACS Nano* **10**, 4797–4805 (2016).
14. Wang, S., Lin, L. & Wang, Z. L. Nanoscale triboelectric-effect-enabled energy conversion for sustainably powering portable electronics. *Nano Letters* **12**, 6339–6346 (2012).
15. Wang, S. *et al*. Sliding-triboelectric nanogenerators based on in-plane charge-separation mechanism. *Nano Letters* **13**, 2226–2233 (2013).
16. Wang, S., Niu, S., Yang, J., Lin, L. & Wang, Z. L. Quantitative Measurements of Vibration Amplitude Using a Contact-Mode Freestanding Triboelectric Nanogenerator. *ACS Nano* **8**, 12004–12013 (2014).
17. Wang, S., Xie, Y., Niu, S., Lin, L. & Wang, Z. L. Freestanding triboelectric-layer-based nanogenerators for harvesting energy from a moving object or human motion in contact and non-contact modes. *Adv. Mater.* **26**, 2818–2824 (2014).
18. Lin, Z. *et al*. Large-Scale and Washable Smart Textiles Based on Triboelectric Nanogenerator Arrays for Self-Powered Sleeping Monitoring. *Adv. Funct. Mater.* **28**, 1704112 (2018).
19. Wang, Z. L., Chen, J. & Lin, L. Progress in triboelectric nanogenerators as a new energy technology and self-powered sensors. *Energy Environ. Sci.* **8**, 2250–2282 (2015).
20. Chen, J. & Wang, Z. L. Reviving Vibration Energy Harvesting and Self-Powered Sensing by a Triboelectric Nanogenerator. *Joule* **1**, 480–521 (2017).
21. Zhu, G., Chen, J., Zhang, T., Jing, Q. & Wang, Z. L. Radial-arrayed rotary electrification for high performance triboelectric generator. *Nat. Commun.* **5**, 3426 (2014).
22. Chen, J. *et al*. Harmonic-resonator-based triboelectric nanogenerator as a sustainable power source and a self-powered active vibration sensor. *Adv. Mater.* **25**, 6094–6099 (2013).
23. Jin, L. *et al*. Self-Powered Safety Helmet Based on Hybridized Nanogenerator for Emergency. *ACS Nano* **10**, 7874–7881 (2016).
24. Yang, W. *et al*. Harvesting Energy from the Natural Vibration of Human Walking. *ACS Nano* **7**, 11317–11324 (2013).
25. Zhu, G., Bai, P., Chen, J. & Wang, Z. L. Power-generating shoe insole based on triboelectric nanogenerators for self-powered consumer electronics. *Nano Energy* **2**, 688–692 (2013).
26. Hou, T.-C. *et al*. Triboelectric nanogenerator built inside shoe insole for harvesting walking energy. *Nano Energy* **2**, 856–862 (2013).
27. Lin, Z. *et al*. Triboelectric Nanogenerator Enabled Body Sensor Network for Self-Powered Human Heart-Rate Monitoring. *ACS Nano* **11**, 8830–8837 (2017).
28. Bai, P. *et al*. Integrated Multilayered Triboelectric Nanogenerator for Harvesting Biomechanical Energy from Human Motions. *ACS Nano* **7**, 3713–3719 (2013).
29. Yang, J. *et al*. Broadband Vibrational Energy Harvesting Based on a Triboelectric Nanogenerator. *Adv. Energy Mater.* **4**, 1301322 (2014).
30. Chen, J. *et al*. Personalized Keystroke Dynamics for Self-Powered Human-Machine Interfacing. *ACS Nano* **9**, 105–116 (2015).
31. Li, Z. *et al*. High-efficiency ramie fiber degumming and self-powered degumming wastewater treatment using triboelectric nanogenerator. *Nano Energy* **22**, 548–557 (2016).
32. Liu, R. *et al*. Shape Memory Polymers for Body Motion Energy Harvesting and Self-Powered Mechanosensing. *Adv. Mater.* **30**, 1705195 (2018).
33. Wang, Z. L. On Maxwell's displacement current for energy and sensors: the origin of nanogenerators. *Mater. Today* **20**, 74–82 (2017).
34. Lin, Z. H., Cheng, G., Lin, L., Lee, S. & Wang, Z. L. Water-solid surface contact electrification and its use for harvesting liquid-wave energy. *Angew. Chem.* **52**, 12545–12549 (2013).
35. Lin, Z. H., Cheng, G., Lee, S., Pradel, K. C. & Wang, Z. L. Harvesting water drop energy by a sequential contact-electrification and electrostatic-induction process. *Adv. Mater.* **26**, 4690–4696 (2014).
36. Tang, W. *et al*. Liquid-Metal Electrode for High-Performance Triboelectric Nanogenerator at an Instantaneous Energy Conversion Efficiency of 70.6%. *Adv. Funct. Mater.* **25**, 3718–3725 (2015).
37. Zhao, X. J., Zhu, G., Fan, Y. J., Li, H. Y. & Wang, Z. L. Triboelectric Charging at the Nanostructured Solid-Liquid Interface for Area-Scalable Wave Energy Conversion and Its Use in Corrosion Protection. *ACS Nano* **9**, 7671–7677 (2015).

38. Lin, Z. H. *et al*. A multi-layered interdigitative-electrodes-based triboelectric nanogenerator for harvesting hydropower. *Nano Energy* **15**, 256–265 (2015).
39. Lee, J.-W. & Hwang, W. Theoretical study of micro/nano roughness effect on water-solid triboelectrification with experimental approach. *Nano Energy* **52**, 315–322 (2018).
40. Lee, K. *et al*. A spherical hybrid triboelectric nanogenerator for enhanced water wave energy harvesting. *Micromachines* **9**, 598 (2018).
41. Kim, T. *et al*. Design and optimization of rotating triboelectric nanogenerator by water electrification and inertia. *Nano Energy* **27**, 340–351 (2016).
42. Zhao, X. J., Kuang, S. Y., Wang, Z. L. & Zhu, G. Highly adaptive solid−liquid interfacing triboelectric nanogenerator for harvesting diverse water wave energy. *ACS Nano* **12**, 4280–4285 (2018).
43. Liang, Q. *et al*. Highly transparent triboelectric nanogenerator for harvesting water-related energy reinforced by antireflection coating. *Sci. Rep.* **5**, 9080 (2015).
44. Zheng, L. *et al*. Silicon-based hybrid cell for harvesting solar energy and raindrop electrostatic energy. *Nano Energy* **9**, 291–300 (2014).
45. Wang, J. *et al*. Water energy harvesting and self-powered visible light communication based on triboelectric nanogenerator. *Energy Technol.* **6**, 1929–1934 (2018).
46. Lee, J. W. *et al*. Pump drill-integrated triboelectric nanogenerator as a practical substitute for batteries of intermittently used devices. *Nano Energy* **56**, 612–618 (2019).
47. Niu, S. *et al*. Theory of Sliding-Mode Triboelectric Nanogenerators. *Adv. Mater.* **25**, 6184–6193 (2013).
48. Lyu, S. & Hwang, W. Selective superhydrophilic/phobic coating using capillary pressure for positive-displacement nanoliter dispensing. *Surf. Coat. Technol.* **277**, 258–261 (2015).

Acknowledgements

This research was supported by the Agency for Defense Development in Korea [grant number UE161007RD] and the National Research Foundation of Korea (NRF) through a grant funded by the Korea Government (MSIT) [grant number NRF-2016R1A2A1A05005414].

Author contributions

H.R. Park and J.W. Lee have an equal contribution of conducting experiments and writing the manuscript. D.S. Kim motivated H.R. Park and J.W. Lee to materialize the concept idea. J.Y. Sim advised and helped the authors with understanding fundamentals of electrical phenomenon and circuit. I. Song helped with conducting precise experiment and improving manuscript. W. Hwang directed the total paper and experimental works. All authors reviewed the manuscript.

Competing interests

The authors declare no competing interests.

Additional information

Supplementary information is available for this paper at https://doi.org/10.1038/s41598-020-57851-9.

Correspondence and requests for materials should be addressed to W.H.

Reprints and permissions information is available at www.nature.com/reprints.

Publisher's note Springer Nature remains neutral with regard to jurisdictional claims in published maps and institutional affiliations.